Search for low-mass objects in the globular cluster M4. I: Detection of variable stars.

M. Safonova[1] and D. Mkrtichian[2] and P. Hasan[3] and F. Sutaria[1] and N. Brosch[4] and E. Gorbikov[4] and P. Joseph[5]

Indian Institute of Astrophysics, Bangalore 560034, India

NARIT, Thailand

Maulana Azad National Urdu University, Hyderabad

Tel Aviv University, Tel Aviv, Israel

Christ University, Bangalore, India

ABSTRACT

With every new discovery of an extra-solar planet, the absence of planets in globular clusters (GCs) becomes more and more conspicuous. The null detection of transiting hot Jupiters in globular clusters 47 Tuc, omega Cen and NGC6397 presents an important puzzle, raising questions about the role played by cluster metallicity and environment on the survival of proto-planetary systems in a densely populated stellar clusters. GCs were postulated to have many free-floating planets, for which the microlensing (ML) is an established tool for detection. Dense environment, well-constrained distances and kinematics of lenses and sources, and photometry of thousands of stars simultaneously make GCs the ideal targets to search for the microlensing. We present preliminary results of a multi-site, 69-nights long, campaign to search for ML signatures of low-mass objects in the globular cluster M4, which was chosen due to its proximity, location and existence of a planet. While no high-significance ML event was found in this observational run, we have detected more than twenty new variables and variable candidates in the M4 field, which we describe in this paper.

Subject headings: globular clusters: general — globular clusters: individual (M4) — stars: variables: general — microlensing

1. Introduction

The field of exoplanetary studies has evolved considerably over the past few decades and is now one of the fastest developing sciences, with 1800 planets confirmed and more than 4,000 candidates discovered since 1995[1]. It is now believed (Cassan et al. 2012) that stars with planets are a rule rather than exception, with estimates of the actual number of planets exceeding the number of stars in our Galaxy alone by orders of magnitude (including unbound, or free-floating, planets, e.g., Strigari et al. 2012); super-Earths being the most abundant type. Our interest in exoplanets lies in the fact that since, antropically, we believe that life can only originate and exist on planets; therefore the most fundamental interest is in finding the habitable planet — the Earth twin.

However, with every new discovery of an extrasolar planet in the field of the Galaxy, the paucity of planets in stellar clusters becomes more and more conspicuous. Given that most exoplanet searches rely on repeated scans of a strip of the local sky, there is certainly a selection bias, ensuring that nearly all of exoplanets (and exoplanet candidates) detected so far reside in the field of the Galaxy. However, the theoretical models, realistic N-body cluster Monte Carlo simulations, including realistic estimates of the binary fraction, the

[1]E-mail: rita@iiap.res.in

[1]Extrasolar Planets Encyclopedia, http://exoplanet.eu/catalog/

two body relaxation, binary and single star evolution, strong encounters, and Galactic tidal stripping (Chatterjee, S. et al, 2012) suggest otherwise. In the case of the open cluster (OC) NGC 6791 in the it Kepler field of view (FOV), these authors find that 10 to 20 planets should be detectable, to limiting magnitude of $K_P < 20$ over the time span of the mission. This simulation assumed that the actual distribution of planets in the cluster is identical to that observed in the rest of the it Kepler field. Thus, although most stars, including our Sun with its large planetary system, are born in stellar clusters, the scarcity of detected planets in both OCs and GCs presents an important puzzle. Is environment important for formation and/or survival of planets? The usual reasons that are brought forward to explain the lack of cluster planets are high stellar densities leading to high interaction rate and disruption of forming planetary systems, or even inhibition of planetary formation due to the truncation of protoplanetary disks (see e.g. Rosotti et al. 2014 and references therein). UV photoevaporation and SNe/stellar winds have also been suggested to inhibit and/or disrupt planetary formation (e.g. Bally 2003, Adams et al. 2004).

Null results in the dedicated searches in GCs 47 Tuc, ω Cen and NGC 6367 (Gilliland et al. 2000; Weldrake et al. 2007, 2008; Nascimbeni et al. 2012) and only a handful of planets in OCs (Mochejska et al. 2006, Montalto et al. 2011) seem to confirm these theories. However, the recent findings from the observations of the OC NGC 6811 (Meibom et al. 2013) have turned the tide. The main conclusion of the study, based on the *Kepler* data, is that the frequency of stars with planets in OCs is consistent with the frequency of stellar hosts in the Galactic field. It shows that the planets can indeed survive the harsh conditions of the cluster's early dense phase, SNe explosions, UV radiation and stellar winds from young stars. Moreover, the existence of planets in multiple host systems (at least 57 planetary systems as of 2012, Roell et al. 2012) indicates that neighboring stars perturbations do not efficiently inhibit formation of planets. *Kepler*'s discoveries of multiple planets orbiting multiple hosts shows that such systems are common in the Galaxy (e.g. Di Folco et al. 2014, Horch et al. 2014, Roberts et al. 2015).

1.1. Planets in GCs

In globular clusters, another reason for the absence of planets was proposed — low intrinsic metallicities of most Galactic GCs. However, metal-rich OCs NGC6791 ([Fe/H]=0.3) and NGC 6940 ([Fe/H]=0.3) were the subject of a number of transit surveys with null results, while a relatively metal-poor GC M4 ([Fe/H] ~ -1.2) hosts a planet. Schekinov et al. (2013) proposed that the so-called "metallicity effect" — higher frequency of planets around metal-rich stars — is most probably a selection effect in that most stars surveyed for a transit are nearby stars in the metal-rich neighborhood of the Sun. In addition, hot Jupiters seem to have strong dependence on host metallicity (Fisher et al. 2004) and the search for planets in GCs was designed to only look for hot Jupiters. Hot Jupiters are a very special type of planets, orbiting at distances of less than 0.1 a.u. and tidally locked to the parent star, thus the GC planets surveys were biased to detection of only the close-in planets. In the solar neighbourhood $\sim 1-2\%$ of solar-type stars have hot Jupiters. The searches in 47 Tuc and ω Cen were based on the assumption that if GCs have the same distribution of hot Jupiters as the field stars, the probability of detecting a transit would be $\sim 10\%$. However, GCs have more evolved stars rather than sun-like; K or M spectral types with $\sim 0.8\ M_{\odot}$mass on average. In addition, transit methods are fraught with limitations such as stellar noise — low-level variability, dependence on line-of-sight orientation and necessity to observe several transits for the firm confirmation. Kepler's mission was successful as it was looking at nearby stars — most of the planets Kepler detected reside typically between about 100 pc and 1 kpc, while the distance to 47 Tuc is ~ 5 kpc, to ω Cen is 4.8 kpc and to NGC 6397 about 2.2 kpc. In summary, hot Jupiters in old GCs do not form because of low metallicity. If they form, they would form at large radii from their low-metal hosts (Soker and Hershenhorn 2007). But most wide-separation systems (> 0.3 au) will be disrupted due to tidal interactions with neighbouring systems which is expected to be very effective in dense GCs (Bonnell 2000). Therefore, search for hot transiting Jupiters is generally futile in GCs. Debes and Jackson (2010) suggested that different search strategy should be employed to look for transits in GCs. Extending the search

to many more cluster members, with longer observational windows and increased observational accuracy may yet yield the planetary

1.2. Free-Floating Planets

Out of all exoplanets, free-floating planets (FFPs) — planets attached to no star, are especially interesting, because, like cosmic wanderers, they may be the source of life, spreading seeds of life throughout the Galaxy (e.g. Stevenson 1998, Durand-Manterola & Javier 2010). According to recent estimates (Strigari et al. 2012), their number in our Galaxy may exceed the number of bound planets and free-floating planets are expected to be a common product of most planetary formation scenarios (Bennet et al. 2007). A large population of FFPs in the Galaxy may contribute significantly to the unresolved diffuse infrared background (Dado et al. 2011) or even to the galactic baryonic dark matter content (Gibson & Schild 1999; 2009), explaining the small $\sim 1:10$ mass ratio between gas and stars in the Milky way (Fukugita and Peebles, 2004). Daily flares detected in the vicinity of the Milky Way central black hole could be attributed to the regular destruction of planets and asteroids (Zubovas et al. 2011), implying a huge amount of planetary/asteroid size bodies at the centre of the Galaxy.

In clusters, tidal disruption of planetary systems (see Spurzem et al. 2008 and references therein) would lead to a population of FFPs. Simulations by Parker and Quanz (2004) have shown that planetary systems with large a ∼5-30 a.u. are likely to be disrupted by close passages of neighbouring stars in the birth clusters at a rate of up to ∼10%. Using N-body simulations, Hurley and O'Shara (2007) showed that as much as 30% of planets in a typical GC could get liberated from their parent stars. A population of free-floating sub-stellar objects has been detected in young open clusters (see for ex. Lucas et al. 2001, Zapatero-Osorio et al. 2002; Haisch et al. 2010; Ramírez et al. 2011), which are more likely formed like stars but reside in planetary mass range. Ramírez et al. (2012) have recently identified a population of planetary-mass objects in the σ-Ori cluster and suggested that they could be as numerous as brown dwarfs. It also indicates that there could be a population of such objects in the solar vicinity, both in the field and in young moving groups and clusters. In 2012, a 4–7 Jupiter-mass free-floating planet was discovered at 30 pc from Earth, belonging to the young moving group AB Doradus (CFBDSIR2149-0403, Delorme et al. 2012), and in 2013, a 6 Jupiter-mass FFP at 24 pc from Earth, in Beta Pictoris moving group (PSO J318.5-22, Liu et al. 2013).

1.3. FFPs formation channels in GC

Several channels exist for FFP formations. FFPs of Jupiter-mass can form by collisions between high-mass protoplanetary disks if the stellar densities are high (Lin et al. 1998), as is the case in GCs. They could be scattered from already formed planetary systems by dynamic interactions in the multiple-planet system or in multiple-star systems (e.g. Veras and Raymond 2012, Ford 2014), or kicked out by interaction of the system with a passing star, especially if they reside at large orbital separation. They could have been kicked out from the system during parent star's mass loss in the end of stellar life (Veras et al. 2011), especially planets as orbitally distant as several hundred AU. Planets could have been formed *in situ* by direct collapse like stars or from the cometary blobs (CB) – remnants of SNe explosions as suggested by Dado et al. (2011) and could represent the low-mass tail of the stellar IMF (Veras and Raymond 2012).

Several circumstantial pieces of evidence point to existence of planets in GCs:

1. Demonstration by Ida and Kakubo (2001) that protoplanetary disks with lower than solar metallicity can form many terrestrial planets, perhaps as many as 50-100 per star (Hurley and Shara 2001).

2. Report that the so-called 'second parameter' problem of the horizontal brach (HB) morphology in GCs can be resolved by assuming the 'planet second parameter' model, where the planetary formation in GCs can in fact be very efficient at the time the GCs were forming (Soker and Hadar 2001). Incidentally, the authors noted that 47 Tuc would not have hot Jupiters due to the paucity of blue HB stars in that cluster, and that the clusters with a high value of HBR index shall

be expected to have planets around many MS stars.

3. Association of several previously detected ML events in the bulge with few GCs (de Luca and Jetzer 2008). It was shown that the modeling does not rule out lensing of the bulge stars by the sub-stellar objects in these clusters.

4. An absence of an obvious correlation between the metallicities of the host star and the presence of low-mass planets (Buchhave et al. 2012).

5. Existence of planets orbiting metal-poor old stars; sometimes as old as 11.2±1.0 Gyr (e.g. Kepler-444, Campante et al. 2015).

6. Actual existence of a planet in a metal-poor GC M4 — PSR B1620-26 b. This planet was probably formed through gravitational instability in a circumbinary disk of a PSR-WD progenitors as a result of an interaction with a passing MS star — the formation scenario which is insensitive to the metallicity (Beer, King and Pringle 2004).

7. A discovery of a Li-rich star in M4 (Monaco et al. 2012). One possible explanation of a Li content higher than normal for Pop. II stars was recently suggested for the case of a red giant field star BD+48740 (Adamow et al. 2012), which has at least one planet, — that a star ingested a planet. Li is preserved in relatively cold environments of planets as they form. A planet absorbed by a star would deliver lithium to its atmosphere. Primordial level of Li in an M4 star #37934 could be a hint towards it, which would mean that the star has (or had) planet(s).

8. Demonstration by observational analysis and theoretical modelling that a hard X-ray transient near the centre of the GC NGC6388 is strongly consistent with a tidal disruption of a free-floating terrestrial planet by a massive white dwarf (Del Santo et al. 2014).

2. Microlensing in Globular Clusters

Since FFPs are not bound to a star, they are undetectable by any of the traditional searching methods, transit or radial velocity (RV), thus it is necessary to employ other techniques. Gravitational ML is already established as an additional tool in detecting extra-solar planets. Unlike the usual RV or transit methods, it is sensitive to low-mass planets or even multiple-planetary systems, such as the Solar System (Gaudi et al. 2008), moreover, ML is the only way to detect the population of FFPs in GCs as their direct imaging is not possible.

First free-floating planets have been detected by the ML in 2011 (Sumi et al. 2011), which was the basis for the Strigari et al. (2012) estimates. However, ML method to search for planets is not devoid of difficulties due to several factors. At any time, only some out of, for example, $\sim 10^6$ Galactic bulge stars, are microlensed with sufficient magnification and, if such an event is due to a foreground planet, it is usually of a very short duration due to a small planetary $R_{\rm E} \sim 1$ day even for a giant planet ($M \sim 10^{-3}\ M_{\odot}$), and duration decreases as $\sqrt{M_{\rm planet}}$, thus demanding a very high cadence (it may change with the launch of a Microlensing Planet Finder MPF, Bennet et al. 2010). However, there is still a problem of a mass-distance degeneracy. ML observations allow the measurement of only two observables, the timescale of the event and the amplification at maximum. The timescale of the event $t_{\rm E}$ is defined as the time it takes a source to cross the Einstein radius $R_{\rm E}$ of the lens

$$t_{\rm E} = \frac{2R_{\rm E}}{v_{\rm t}} = \frac{4}{v_{\rm t}c}\sqrt{\frac{GM_{\rm L}D_{\rm L}\left(D_{\rm S}-D_{\rm L}\right)}{D_{\rm S}}}\,. \qquad (1)$$

Here $M_{\rm L}$is the lens mass, $D_{\rm L}$ and $D_{\rm S}$ is the the observer-lens and observer-source distance, respectively, $v_{\rm t}$ is the lens transverse (to the line-of-sight) velocity and the Einstein radius $R_{\rm E}$ defines the region of high amplification. In most cases the lens is not seen and therefore, D_L cannot be independently determined. If, for example, one has measured a certain timescale of one month, it could be either due to large lens mass and small lens velocity, or small lens mass and large lens velocity. Several methods were suggested and are being used to resolve this degeneracy, which essentially requires the breaking of the symmetry of a standard Paczynski light curve (see e.g. review in Sutherland 1999, but not exclusively). For long-timescale microlensing events

(months or year(s)), it is frequently possible to measure the microlensing parallax effect (Gould 1992; Alcock et al. 1995), where diurnal motion of the Earth distorts the usually symmetric around the maximum light curve. As the orbital motion of the Earth is well known, degeneracy in this event could be broken and it may be possible to estimate $D_{\rm L}$, $v_{\rm t}$, or both (e.g. Nucita et al. 2006). Another possibility is when the source size is comparable to the Einstein ring of the lens breaking the point-source-point-lens approximation and also resulting in a deviation from the symmetric microlensing curve — a finite source effect. In such case, it is possible to determine the angular size for the source and thus the mass of the lens (e.g. Rattenbury & Mao 2005).

Here, we suggest that observing globular clusters for the ML by FFPs belonging to the cluster can, in principle, resolve this degeneracy and, with carefully arranged observational setup, such planets can be detected from the ground. GCs present ideal targets for dedicated ML searches — their compactness allows observations of thousands of stars in a single exposure in a single frame, which maximizes the temporal coverage and increases the probability of detection. Events produced by planetary lenses are of only $\sim$ few days for a giant planet (see Sec. 3), therefore it is sufficient to observe a cluster for several consecutive nights. A good general knowledge of GCs — stellar kinematics, metallicity, ages and distances, relative inhomogeniety in many parameters and a history of formation from the same initial cloud (same IMF) provides means of resolving the mass-distance degeneracy, offering the only possibility to constrain their numbers and masses. Though the Einstein radius of an FFP event is small (the probability of a detectable planetary signal and its duration scale as the Einstein radius), given the perfect alignment, ML signal — the high-amplification event — even from low-mass planets can be quite strong.

Free-floating planets behave like low-mass stars evaporating into the cluster's halo, especially in the presence of strong tidal interactions (Spurzem et al. 2009) while passing through the Galactic plane. Fregeau et al. (2002) performed the numerical simulations of the mass segregation in two-component star clusters and found that low-mass objects in the cluster halo can dominate the ML optical depth — for some initial conditions, the optical depth in the halo could be much greater than that of luminous stars. Many GCs are known to exhibit tidal trails and haloes (e.g., Leon et al. 2000) and it is possible that these trails contain FFPs or low-mass stars with their planets still orbiting. In 2014, two planets were found orbiting a metal-poor Kapteyn's star (Anglada-Escud'e et al. 2014), which most probably belongs to the tidal tail of the ω Cen (Wylie-de Boer et al. 2010). The planet in M4 is also estimated to lie outside the half-mass radius of the cluster (Beer et al. 2004).

3. Target Cluster

M4 (NGC 6121) is the closest globular cluster to the Sun at $\sim$ 2.2 kpc. It is a very bright (V=5.9 mag), relatively sparse, relatively metal-poor ([Fe/H] ~ -1.2) cluster projected near the edge of the Galactic bulge. The line of sight to M4 passes through the Galactic inner halo, or perhaps more correctly, the inner Population II spheroid, and the distant field stars may belong to the bulge or inner halo. The far side of the galactic bar is also projected into the same Galactic quadrant as M4. We expect only a small number of foreground disk stars in our field, but there is a large number of background stars that can serve as sources for ML event.

M4 is an interesting cluster in several ways. First, it hosts the only planet ever discovered in a globular cluster, a PSR B1620-26 b (Richer et al. 2003). Secondly, the high ratio of a cluster age to the half-mass relaxation time strongly suggests that the cluster had experienced a core collapse, of which, however, there is no observational evidence (Richer et al. 2004). Therefore, M4 is expected to have an internal energy source capable of preventing core collapse. One candidate for this is primordial binaries, though the detected fraction of such objects is very low. The central M4 binary fraction is $\sim$2% as compared to $\sim$5.1% in the the similar in most parameters NGC 6397 (Richer et al. 2004, Davies et al. 2008), or to $\sim$22% and $\sim$21% in prototypical core-collapse clusters M71 and NGC 362, respectively.

M4 has a well-developed mass segregation (Richer et al. 2004) and a highly eccentric (0.88, Allen&Santillan, 1993) chaotic orbit with Galactocentric distance ranging from 0.5 to 6.9 Kpc at each passage, resulting in M4 population being

strongly affected by tidal interactions with the Galactic disk. Due to the strong tidal stripping, M4 is expected have a low-mass star deficiency. However, Richer et al. (2004) have calculated the number of stars at the hydrogen limit 0.085 $M_{\odot}$to be from 14–49 with the conclusion that if the slope of cluster's mass function is unchanged down the end of the main sequence (MS), then there should be at least a few tens of MS stars at the faint end of M4 field. They, however, found only six at $M \simeq 0.1 M_{\odot}$ (Richer et al. 2004). The existence of a minimum stellar mass is a fundamental theoretical result that can in principle be confirmed by ML.

Since the cluster is situated very close to us, the majority of objects of interest would most probably belong either to M4 or to the bulge, therefore we consider only these locations. To determine the cadence of observations, we assume that the lens belongs to the cluster and calculate the time scales of possible planetary ML events for two scenarios: A) the source is a bulge background star and B) the source is a star within the cluster — a case of self-lensing. The relevant parameters for M4 are presented in the Table 1.

Table 1: Relevant parameters of M4.

Distance from the Sun $D_{\rm L}$	1.8 Kpc
Central velocity dispersion σ_0	4 km/sec
Proper motion $\dot{\phi}$	23.4 mas/yr
Diameter $D_{\rm GC}$	42 pc
Distance to the bulge $D_{\rm S}$	8.2 Kpc

Case A.

Estimates of the predicted number of events in Galactic GCs were given in Paczyński (1994), and more recently in Jetzer et al. (2015) where four possible ML events were associated with the lenses in the clusters seen against the background of the Galactic Centre. See Jetzer et al. (1998) for detailed calculations. Following Paczyński (1994), the equation for the ML time scale in this case is:

$$t_{\rm E}(d) = 32.4 \left(\frac{M_{\rm L}}{0.1 M_{\odot}}\right)^{1/2} \times \left(\frac{1\,kpc}{D_{\rm L}}\right)^{1/2} \times \left(1 - \frac{D_{\rm L}}{D_{\rm S}}\right)^{1/2} \times \left(\frac{10\,mas/yr}{\dot{\phi}}\right) . \quad (2)$$

Here $\dot{\phi}$ is the cluster's proper motion relative to the background stars. We assume that the lensed object is in the galactic bulge at a typical distance of 8.2 kpc. We then consider the following three lens mass scenarios: a low-mass star with 0.1 $M_{\odot}$, a brown dwarf with 0.07 $M_{\odot}$, and a hot Jupiter with $M = 0.001\ M_{\odot}$. From Eq. (3), we estimate $t_{\rm E} = 8.65$ days, 7.33 days, and $\sim$ one day, respectively.

Case B.

The self-lensing in globular clusters was discussed in Safonova & Stalin (2010). The equation for the time-scale is

$$t_e = 48.6 \left(\frac{10\,{\rm km/sec}}{\sigma}\right) \left(\frac{M_{\rm L}}{M_{\odot}}\right)^{1/2} \left(\frac{D_{\rm LS}}{1{\rm Kpc}}\right)^{1/2} , \quad (3)$$

where $D_{\rm LS}$ is the lens–source distance which we take to be the diameter of the cluster, $D_{\rm GC}$. For the same three cases as discussed in Case A, we find the following time scales: 7.87 days for a low-mass star, 6.65 days for a brown dwarf and about 19 hours for a hot Jupiter.

Given these values, it was decided to perform photometric monitoring of the cluster for about 4 months several times a night. As the lensing curves are achromatic, to distinguish from variations due to other phenomena, we carried out observations in two filters (I and R-band) several times a night (when possible) in short exposures to avoid saturation of bright cluster stars. In addition, observing M4 with a wide-field telescope, with FOV larger or at the tidal radius ($\sim 22'$), offers the opportunity to search for FFPs in its halo, especially with a background rich in stellar objects. Keeping that in mind, we have supplemented the T40 observations with 6 nights on a wide-field C18 telescope with FOV=75 $\times$ 50 arcmin – a total area of > 1 square degree.

To extract the photometric variability we have employed the differential imaging analysis (DIA) which showed excellent results when applied to the large data sets, and especially in dense stellar fields (e.g. Alard and Lupton 1998, Wozniak et al. 2000). DIA is sensitive to ML events even when the source star is too faint be be detected at the baseline. We expect no light contribution from the lens and, providing foreground stars are constant, the contribution of any foreground star

will be cancelled out in delta flux (ΔF, Eq. 5) measurements. In DIA, if there is no difference in flux between the images, the residual frames are theoretically flat. A variable/transient source will show up as positive or negative on the residual frames (Eq. 4), which can be easily detected.

$$\Delta F = F_{\rm base} A\left(u(t)\right) - F_{\rm ref}\,, \qquad (4)$$

where $F_{\rm base}$ is the baseline (unmagnified) flux of a star undergoing amplification, $F_{\rm ref}$ is the flux of that star on a reference frame, and $u(t)$ is the time-dependent impact parameter – the distance between the source and the lens in terms of Einstein angle. Amplification governs the shape of the ML light curve,

$$A\left(u(t)\right) = \frac{u^2+2}{u\sqrt{u^2+4}}\,. \qquad (5)$$

High amplification events occur when u is small $u \ll 0.05$. For $0.05 \leq u \leq 0.02$, amplification can be 20 to 50, corresponding to a maximum increase in brightness of 2 to 4 magnitudes.

4. Observations

Main observational run was performed with 1-m telescope (T40) of WISE Observatory, Tel Aviv, Israel, from 06 April to 07 July 2011 in service mode, gathering 12 to 48 20-sec exposures a night for a total of 69 nights in R and I filters. We have used R and I because the the CCD's QE is $\sim 40\%$ between R and I and only about half of that in V. The field analyzed here is one out of four LAIWO mosaic CCDs fields (Fig. 4, *Left*) monitored during the run, CCD chip #2, which itself consists of 4 quadrants (Nos. 5–8) (Baumeister et al. 2006, Gorbikov et al. 2010). The size of each quadrant is 1048×1048 pixels, with a plate scale of 0.87 arcsec/px (equivalent to a total FOV of $\sim 14.5 \times 14.5$ arcmin. The cluster was positioned on the quadrant 8, since it has the best characteristics (Fig. 4 *Right*).

Supplementary observations were performed with the 0.46-m Centurion 18 (C18) telescope, situated in the same area. It is equipped with a large format CCD camera — STL-6303 of SBIG. Observations were performed remotely. The CCD (Brosch et al. 2008) has 3072×2048 with a pixel scale of 1.47 arcsec/pix giving a total FOV of

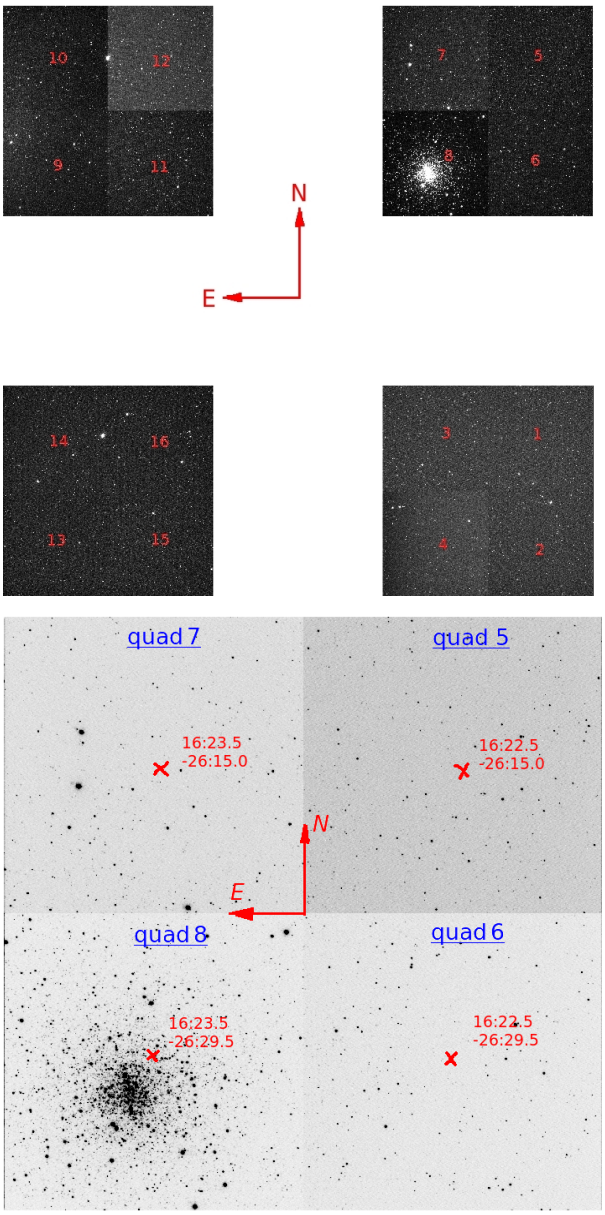

Fig. 1.— *Top*: LAIWO mozaic of M4 field. *Bottom*: LAIWO CCD chip#2 with M4 position on the quad 8.

75×50 arcmin. In the unbinned mode the readout noise is 15 electrons and the gain is 1.379 e/ADU. The observations were done for six nights from 28 May to 02 June, for about 4 hrs each night, gathering a total of 425 60-sec exposures in R and I filters.

5. Data Reduction and Search for Transients

5.1. Basic Data Reduction

5.1.1. T40 telescope

Since the read-out noise and gain were different for each quadrant, we have calibrated them separately. All images were subjected to the basic data reduction (bias subtraction and flat-fielding) using the modular pipeline based on IRAF[2] scripts which is under development by our group. The first module of this pipeline separates the frames based on the CCD image type identifier (bias, flat, object) into the corresponding lists, checks the quality of the images using the image statistics (and rejects the 'bad frames), and edits the image headers with necessary information. The second module performs the basic reduction and creates the lists for the next processing. We did not make a separate dark current correction; the dark current has been found to be negligible for the exposure times used. Flat fields were constructed from dithered images of the twilight sky; the sky flats were also used to correct for large-scale illumination variations in some quadrants (quad 5 and quad 7). The sky flats were used to create the large-scale illumination correction image as follows: the sky flats were combined by finding the median value of each pixel. We removed any star images by combining flats in each colour using a median filter. We did not use the cosmic ray removal module of our pipeline since the Difference Image Analysis Package (DIAPL) we have used in this work[3] has an option for cosmic ray removal at the subtraction stage.

Because the exposure time was only 20 seconds, to increase the signal to noise we co-added up to six images taken sequentially within one hour each night. We thus obtained a time series of frames where one night was represented by one or occasionally up to 4 datapoints. The co-adding was performed using DIAPL code *template.bash*, which assigns the time stamp of the first image of the stack to the final image. After co-adding, the resultant time series were moved to separate directories, one for each filter.

5.1.2. C18 telescope

All images were subject to the same basic data reduction (bias subtraction and flat-fielding) using the same modular pipeline as for T40 telescope, except that we have used the dark current subtraction option in the pipeline. We did not co-add the frames since we were looking for the short-term variability in this run. The pre-processed images were combined by filter and subjected to the same DIAPL in search for variability.

5.2. Search for variability

DIA method is the photometric method specifically designed to work in crowded stellar fields such as GCs (Alard and Lupton 1998). In this method, the so-called reference frame (RF) is constructed from images with the best seeing parameters. Next, a convolution kernel, representing the difference between the stellar point spread functions (PSF) of the RF and all the frames in the time series, is applied to the RF to match each of the images in the series. Finally, a convolved RF is subtracted from from each image in the series. This allows for the elimination of all non-variable stars in the resulting difference frames, while the variable or transient objects show up as positive or negative star-like residuals. The light curves for the variables are then extracted by the application of PSF photometry to the difference frames.

5.2.1. T40 telescope

To reduce the effects of PSF variability, all frames were subdivided at the subtraction stage into overlapping subframes, depending on the number of stars in each quadrant. Quad 5 was not split at all, quad 6 and quad 7 were split into 2×2 subdivisions (524×524 pixel size) and quad 8 (where most of the cluster was located) was split into into 5×5 (209×209 pixel size) and into 4×4 (262×262 pixel size) subframes, as in the first case we found that some variables were lost between the subframes borders.

Reference frames for each quadrant were constructed by combining several (depending on the quadrant) co-added images with good seeing and

[2]IRAF is distributed by the National Optical Astronomy Observatory, which is operated by the Association of Universities for Research in Astronomy, Inc., under a cooperative agreement with the National Science Foundation.

[3]We have used the version of DIAPL (Wozniak 2000), modified by W. Pych. This package is available at `http://users.camk.edu.pl/pych/DIAPL/`.

low background. The combined frames were remapped to the RF coordinate system and the convolved RF was subtracted from each frame in the time series (for details of the algorithm, see Wozniak 2000). The residual frames (difference images) were searched with IRAF DAOFIND for the presence of any positive stellar-like residuals, each subdivision separately. Regions at the locations of saturated stars were masked to remove them from the search. Since the stars undergoing the light variation show different brightness on each of the residual images, it was difficult to determine their central coordinates accurately; there was a slight constant positional variability of their PSF. To solve this problem, the pixel coordinate lists of detected residuals on every frame were 'dumped' into one total list (IRAF *txdump*). Each source was assigned a unique ID number by DAOFIND and we used this ID for all subsequent lists and databases. Concatenation of the coordinates from each subtracted frame was done by a fortran code which searched for the nearest neighbours (within a specified radius of, say, 5–10 pixels) and averaged the centroid. The DIAPL photometry was performed on this final coordinate list, the light curves were extracted in units of difference counts on subtracted images and examined by eye. The coordinates of the stars whose light curves were showing possible interesting variation were fed into the IRAF task PHOT to extract their aperture photometry on the reference frames. These measurements were used to obtain the light curves in instrumental magnitudes by DIAPL.

For the light curves in which light variation was found, several methods were employed to find the best fitting period: phase minimization method (PDM) using IRAF (*astutil* package), period determination code based on the Lomb-Scargle (LS) method and the power spectrum analysis (Press et al. 2007), where the LS period is subsequently passed on to the code based on algorithm of Lafler & Kinman (1965) (LK method), and the light curves are phased out. Final analysis was performed using the open source PerSea 2.1 package (Maciejewski 2005), which is based on the optimal analysis of variance period search method of A. Schwarzenberg-Czerny and allows the automated variability type assignment.

5.2.2. C18 telescope

The image frames were split into 8×6 subdivisions (424×324 pixel size) and RFs in both filters were constructed from only 9 best frames from 29th May, to minimize the chance of having a ML event in these frames. The rest of the methodology was as for the T40.

6. Astrometric and Photometric Calibration

6.1. T40 telescope

Astrometric solution of each quadrant's RF was performed using two methods. Each quadrant's reference frames were loaded into Aladin Sky Atlas (Bonnarel et al. 2000) with a corresponding field from HST catalogued images and bright, but not saturated, stars were matched between the frames. We have used about 26 stars from all over the field and far from the centre to perform this transformation. Each thus calibrated RF was checked by loading the all-sky catalogues PPMXL (Röser et al. 2010,http://vo.uni-hd.de/ppmxl) and 2MASS (Skrutskie et al. 2006) catalogues and for all quadrants but quad 6, the accuracy was within 1 arcsecond. Quad 6 was rotated and scaled down; therefore for this quadrant we have used IRAF astrometric calibration utility. No less than 20 standard stars from the online catalogue by P. Stetson (2000) at the Canadian Astronomical Data Center (CADC)[4] uniformly distributed around the quadrant centre were identified and the list of their (x,y) and (RA, Dec) coordinates was created. This list was an input to the *ccmap* task of the *imcoords* package in IRAF. The obtained accuracy was $0''.0678$ in RA and $0''.0437$ in Dec. The task *ccsetwcs* was used to update the header of the quad 6 RF in J2000 epoch.

The same Stetson's photometric standards were used to obtain the absolute photometric calibration. For stars whose standard R magnitudes were not available in Stetson (2000) catalog, data from PPMXL catalogue was used. The photometric solution was obtained by linear fitting the standard magnitudes vs instrumental magnitudes. The resultant solutions (with correlation coefficient of the fit $R \sim 1$) were applied to the instrumental

[4]The catalog is available at http://www3.cadc-ccda.hia-iha.nrc-cnrc.gc.ca/community/STETSON/standards/

magnitudes of variable stars to obtain their standard $< R >$ and $< I >$ magnitudes. In Fig. 2 we show as an example the fit for the quad 5, both I and R filters. We have not found any colour dependence here.

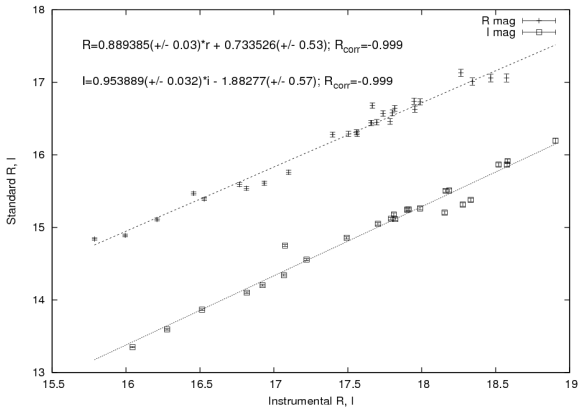

Fig. 2.— Photometric calibration of the quad 5. R and I magnitudes are from PPMXL 2010 catalog.

6.2. C18 telescope

The same approach was applied to the central subdivision 4_3 (Sec. 5.2.1) of the C18 reference frame, except that here we used R and I magnitudes given in Stetson's catalog. The photometric solution was found for 29 Stetson's standard stars and the solution was applied to the instrumental magnitudes of all stars in this subsection. We have found a small colour dependence, which was included in the fitting (Eqs. 6).

$$\begin{aligned} R - r &= -0.167651(R - I) - 0.20271\,, \\ I - i &= -0.137662(R - I) - 0.887425\,, \\ R - I &= 0.861806(r - i) + 0.670682\,, \end{aligned} \quad (6)$$

where R, I are standard magnitudes and r, i are instrumental magnitudes. In Fig. (3) we show the plot of standard deviation (RMS) vs. the mean instrumental r magnitude for this subsection. We used the light curves for all detected ~ 1350 stars in the 4_3 R filter subframe (instrumental magnitudes) of the RF. We can see that our photometric limit is about 19 mag.

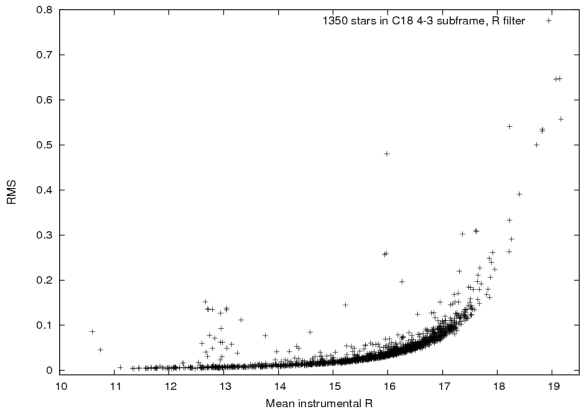

Fig. 3.— Photometric accuracy of the central part of C18.

7. Variability in the Field of M4

7.1. Stars previously reported as variables

M4, being the closest cluster to us, has been a subject of quite an intense attention in the last few years, both from the ground (Kaluzny et al. 2013 and Stetson et al. 2014) and from space (Nascimbeni et al. 2013). In spite of that, few puzzling facts still remain. For example, there are no SX Phe-type stars firmly confirmed in the cluster. Yao (1993) proposed one star as an SX Phe reporting it to be a blue HB star; however, it is located in the wrong place on the cluster's colour magnitude diagram (CMD) and does not seem to even be variable (Yao and Uloa 1993, Stetson et al. 2014). Kaluzny et al. (2013) have reported four SX Phe stars, two cluster members and two field stars; two cluster members were subsequently found to be most probably non-variable and one non-member though confirmed to vary with SX Phe-like period (0.04088 days), to be too faint to be a cluster SX Phe star ($V = 19.3$) (Nascimbeni et al. 2013). Several groups searched for cataclysmic variables (CVs/DNe) and found none. Even the variable blue stragglers (BSS) are only two, one found by Kaluzny et al. (1997), and another only recently by HST observations (Nascimbeni et al. 2013). Although we cannot compete with superior spatial resolution of the HST which detects photometric variability on the order of a few hundredths of magnitude, our present study

complements HST study in having a much wider FOV (see Fig 4). We, in addition, obtained a relatively good photometry in R and I for bright stars, such as cluster's RR Lyrae, a subject of Stetson et al. (2014) study. We also have a time series suited well for investigating both the long periodic variables (LPV, a ∼4 months on T40 telescope) and a short-periodic (SPV, 6 nights on C18 telescope).

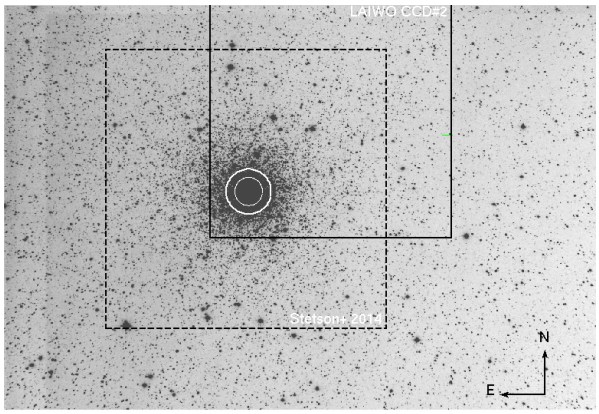

Fig. 4.— R band Reference frame of C18. Overlayed are the FOV of Stetson+ (2014) (dashed black square), LAIWO CCD#2 FOV (solid black square). Small white circle is the FOV of HST study (2014). Solid white circle depicts M4 core size ($r_c = 1.16'$).

Newly updated Christine Clements online catalog (last update 2015, Clement et al. 2001) lists now 111 variables, including recent findings by Kaluzny et al. (2013) from the The Clusters AgeS Experiment (CASE), Nascimbeni et al. (2014) and Stetson et al. (2014).

In this paper we use the variable star identifiers given by Clement et al. (2001). Variables from CASE were named K with some number, and the cross-match with other group's identifiers was performed. In this paper we only report the the newly found variables/variable candidates, and our findings on those previously reported variables that 'brought out something new' (where possible).

We have recovered all variables listed in Clement's catalogue of 2009 (80 variables at the time of observations), except V4, V13 and V53 as they were saturated on both telescopes. In Clement's catalogue, some variables did not have their coordinates defined (V53–V61) (only x, y positions). LAIWO quad8 RF was compared and contrasted to the ID charts of Greenstein (1939), Alcaino (1975) and Lee (1977), and the coordinates of seven variables were located, identified by the assigned name, and their positions were verified. We found their coordinates by triangulating their position on at least two of these ID charts. Their equatorial coordinates were found using Aladin sky atlas and *cctran* task of the *imcoords* package in IRAF with the accuracy $< 0''.1$. These stars with their coordinates and the cross-matches are presented in Table 2.

Incidentally, Stetson et al. (2014) also reported searching for this missing data, and successfully identified them by plotting their predicted positions on their stacked image and finding the closest bright star to each position. They misidentified only one star, V57, and we have confirmed it by verifying with the online Samus et al. (2009) catalog.

7.2. New data on previously reported variables

7.2.1. Non-variable/variable 'variables'

Several stars from the Clement's catalog were suggested to be non-variable in Stetson et al. (2014). To start with, stars V17, V44–V48, V50 and V51, designated as RR Lyrae probably due to their location on the HB of cluster's CMD, were found by Stetson et al. (2014) to be non-variable. We also find stars V17, V45, V46 and V50 non-varying in both our sets; however, stars V44 and V47 show some short-period variation, while V48 and V51 show some long-period variation (Fig. 5). While these last four stars may be varying, they are not of RR Lyrae type based on the shapes of their light curves. We have plotted the light curves in only R magnitude to save space.

Among the non-RR Lyrae stars (V53, V54–V60, V65, V70, V72, V75, V77, V78 and V80) that appear to be either non-variable in Stetson data or their variability is under serious doubt, we also find that V54, V55, V57–V60, V65, V75 and V80 are non-variable in both our sets to the limit of our sensitivity. We cannot comment on V53 as it was saturated in all frames.

Incidentally, stars V51, V56 and V59 were designated as secondary photometric standards (S8, S72 and S94, respectively) in Stetson's (2000) on-

Table 2: Identification of stars V54–V60

Clement ID	Greenstein No.	Alcaino No.	Lee ID	(RA Dec) 2000.0
V54	G30	-	L3621	16:23:42.84 -26:29:28.0
V55	G327	A64	L3315	16:23:45.94 -26:23:37.1
V56	G265	A375	L4508	16:23:45.98 -26:33:39.4
V57	G266	-	L4509	16:23:46.98 -26:33:44.4
V58	G206	A491	L4632	16:23:47.87 -26:32:06.4
V59	G481	A371	L4512	16:23:50.18 -26:33:24.4
V60	G543	A376	L4507	16:23:45.26 -26:33:57.3

line catalog of secondary photometric standards. In fact, stars V56 and V77 deserve special mention. In 2008, a spectroscopic search for binaries in M4 was conducted on the basis of radial velocity variations (Sommariva et al. 2009), where they identified 57 binary candidates. Stars V56 (#29065 in Sommariva et al. 2009) and V77 (#34848 in Sommariva et al. 2009) (= K56 from CASE, see Sec. 7.1) are among this list. In Stetson et al. (2014), these stars are labelled as "EB or LPV" for V56, and "possible EB" for V77, without the periods. We cannot confirm their variability based on our light curves (Fig. 5).

V56 This star was first declared as variable by Yao (1987) based on Greenstein (1939) paper, though neither its coordinates nor period are given in Clement et al. (2001). We found its coordinates (see above Table 2) and discovered that it coincides with Stetson secondary photometric standard S72 (Stetson 2000). It is a RG star, based on its position on the CMD, and a cluster member. In Fig. 5 we show its time-domain light curves from both telescopes.

V77=KV56 Neither Clement et al. (2001) nor Kaluzny et al. (3013) give the period for this star. Kaluzny et al. (2013) presents its time-domain light curve (their Fig. 10), which looks like an LPV. It doesn't look variable on our C18 frames, but its T40 light curve gives indication that it might be an LPV (Fig. 5). Though it could well be decided finally as a binary based on Sommariva et al. (2009) radial velocity variations and Stetson's conclusion, the situation is complicated by its association with X-ray sources CX5 and CX9 (Bassa et al. 2004, Kaluzny et al. 2013). Clearly, more studies have to be done to finalize the issue.

V70 and V72 V70 and V72 variables were found by the HST study (Nasimbeni et al. 2014) to vary as cEB (contact eclipsing binaries) with periods of about 0.3 d. We also find them variable (Fig. 6), with V72 a blue straggler (BSS, see Sec. 7.4.2 and Fig. 14). Interestingly, V70 is reported as RR Lyrae in 2MASS catalog: 2MASSJ16233328-2631079.

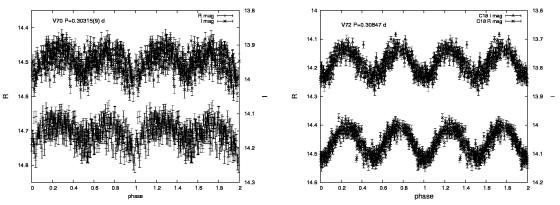

Fig. 6.— C18 phase curves of V70 and V72 in standard R and I magnitudes.

7.2.2. SX Phe stars in M4

SX Phe variables in GCs are of particular interest because they occupy the region on the CMD that coincides with the blue straggler (BSS) region. These stars are believed to be a result of a binary merger. With a slow start (only a handful known in the 90s), the count now exceeds 100 in the galactic GCs, except in M4, which presents an important puzzle, especially that the cluster hosts a large number of BSS stars (30 BSS found by Rucinski (2000) and one more by Nasimbeni et al. (2014). While all SX Phe are blue stragglers, not all blue stragglers are SX Phe. Of all these BSS, only two are variable and both are eclipsing binaries of W Uma type: V72 (Kaluzny et al. 1997)

and #7820 (Nasimbeni et al. 2014).

There are few reports of SX Phe in M4 in the literature. Yao & Uloa (1993) reported a star, which was assumed by Rodriguez & Lopez-Gonzales (2000) as SX Phe in their compilation of then known SX Phe stars in GCs. This star, however, was an outlier in their metallicity-period relation. The star, assigned as V48, not only does not lie in the BSS region of cluster's CMD (in HB, Yao & Uloa 1993), but is even suggested to be non-variable in Clement's catalog. As we mentioned in the previous subsection, it shows some irregular variation in our T40 set, but does look variable in C18 set. Kaluzny et al. (2013) reported four SX Phe stars, two cluster members (K61 and K68) and two non-members (K62 and K64). Stetson et al. (2014) re-examined Kaluzny's data and tentatively found three of those stars to be non-variable and one – a non-member K64 – as variable. HST report (Nascimbeni et al. 2014) studied the central part of the cluster where there should be many SX Phe stars by analogy with other low-metallicity GCs (e.g. M53, M55 or ω Cen) but found none, though they would have been able to detect the variability down to milli-mag amplitudes. They have detected other Kaluzny et al. (2013) variables, such as K48–K51, K53, K66 — all eclipsing binaries. Therefore they should have been able to detect K61 and K68 as SX Phe, if genuine. We examined these stars and conclude that stars K61 and K68 are most probably not SX Phe (Table 3, Fig. (7), which again brings the number of SX Phe in M4 to zero.

7.2.3. RR Lyrae stars in M4

RR-Lyrae stars in the field of M4 from several telescopes have been extensively reported (see Nasimbeni et al. 2014 and Stetson et al. 2014 and). Here we complement that set by reporting on RR Lyrae stars which were outside those FOVs but nevertheless are associated with M4 based on their position on the cluster's CMD and their proper motion.

In quad 5 of LAIWO CCD there is a variable designated as $V12$ in ASAS Variable Stars Catalogue (Pojmanski + 2002-2005) — an RRc, which, however, was believed to be a field variable (Lane et al. 2010). We have obtained its R and I photometry on both telescopes and suspect it to be a cluster member. Firstly, its mean R and I magnitudes are consistent with the mean R and I magnitudes for 45 RR Lyrae in M4 of $\sim$ 12.8 and $\sim$ 12.3, respectively (Stetson et al. 2014). Secondly, its heliocentric radial velocity (HRV) of 64.8 km/s given in ASAS catalog is consistent with the HRV of M4 $\approx$ 69.8 km/s. Finally, in Stetson et al. (2014) the variable V76, that did not have the coordinates in the Clement's catalog, was provisionally identified as RR Lyrae at a cluster distance and the coordinates given therein coincided with the coordinates of $V12$. Therefore, we concur with Stetson's coordinates and confirm the designation of this star as V76, a member of M4 and an RRc variable. Its period in ASAS Catalogue is given as 0.305725 d; we find the best period as 0.305738 d and present its phased R and I light curves in Fig. 8.

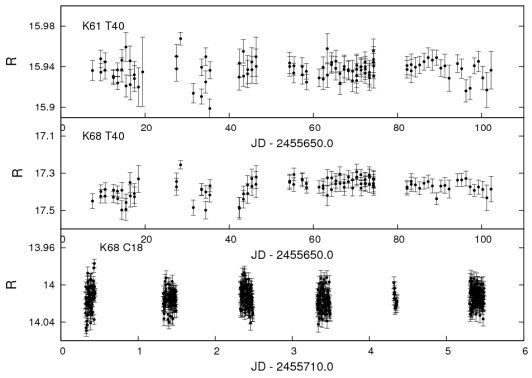

Fig. 7.— T40 and C18 time domain light curves of K61 and K68 in instrumental magnitudes. *Top*: T40 light curves of K61. *Middle&Bottom*: T40 and C18 light curves of K68, respectively.

In addition, three variables were outside Stetson et al. (2014) FOV: V3, V34 and V43. In Fig. 8 we show their light curves, phased with best found periods (Table 4). Variables V3 and V43 were outside the T40 FOV, therefore we have only C18 light curves for them.

Variable V36 is one of the pair of closely separated stars ($3''.6$)of equal brightness (Fig. 9, *Top*). Previous study (Stetson et al. 2014) report noisy light curves for this star. Our T40 light curves were also quite noisy, probably due to the low cadence, therefore we present only C18 light curves (Fig. 8).

Both Stetson et al. (2014) and Nascimbeni

Table 3: SX Phe stars in M4 suggested by Kaluzny et al. (2013)

Kaluzny	P_{Kal}	Stetson+ (2014)	HST study (2014)	This work	
ID	days	result	result	T40	C18
K61	0.0413287	non-var?	did not detect	LP?	blended with bright V=13.165 neighbour; cannot get light curve
K68	0.0380887	non-var?	did not detect	noisy; LP?	not phasing at $P^{\dagger}_{Kal}$

et al. (2014) discovered that previously reported atypical RR Lyrae V40 is in fact a blend of two neighbouring RRc stars of equal brightness, separated by 1″.666. In spite of the limited sensitivity of our photometry and relatively large pixel sizes, we are nevertheless able to distinguish the two stars on the difference frames, most probably due to their large amplitudes and different periods (Fig. 9, *Bottom*). This demonstrates the power of the DIA technique even in the crowded centres of GCs and our ability to detect a high-amplification event if occurred. It was, however, more difficult to obtain high-quality light curves for these two stars because they are so close that their zero-point flux estimate could not been done correctly; the calculated zero-point flux is thus a measurement of the combined flux of these stars. Thus, we could not extract the light curves from C18 as its pixel scale is of the order of separation, and present T40 instrumental R and I phase curves of the lower star (Fig. 8).

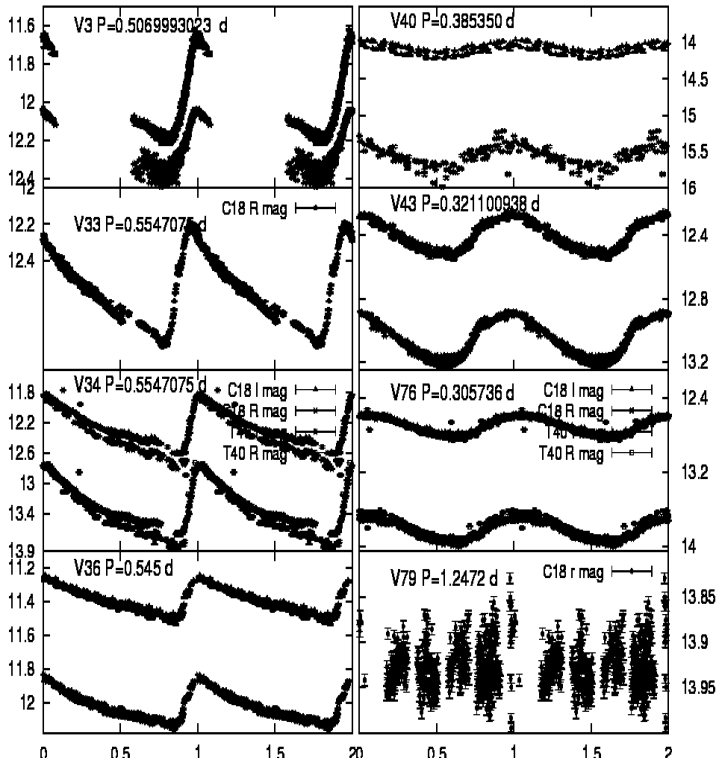

Fig. 8.— C18/T40 light curves of V3, V33, V34, V36, V43, V76 in standard magnitudes. C18 light curves of V40 and V79 are given in instrumental magnitudes (see text). Names and respective periods are given in the plots

7.3. New variables/variable candidates

After examining a set of the candidate variables and rejecting obviously spurious ones, we find 20 new variable stars (Table 5 and Fig. 11) and 7 candidate variables (Table 6 and Fig. 15). The candidates look variable but have noisy light curves that do not allow to certainly detect the periods. In addition, we also detected the C2 variable of Stetson et al. (2014) and, since Stetson et al. (2014) have no R and I data for this star, we include it here with our new detections (Fig. 10, *Top*). In Fig. 11 we present phased light curves of those newly detected variables where we could find the significant period. We present here only R magnitudes to save space.

7.3.1. RR Lyrae

We find several RR Lyrae: 2 RRc (NV8 and possibly NV9), 4 RRab (NV3, NV10, NV13 and C2) and one with undetermined pulsation mode – NV7. One of these stars, NV3, was also detected in Catalina Sky Survey (#J1625293-261718, Torrealba+ 2015) as RRab with the period P=0.48949 d. We find its period as P=0.49178(3) d. Variable C2 was also detected by Stetson et al. (2014); we supplement their discovery with good quality R

Table 4: Data on previously reported variables obtained in this work

Name	$P_{Clement}$ (day)	Present work (day)	$\Delta R/\Delta I$ (mag)	Type/Comments
V3	0.5067	0.50699(9)	0.326/0.533	RRab, $I > R$ amplitude
V33	0.6148	0.61361	0.6834	RRab, R amplitude
V34	0.5548	0.55471	1.062/0.872	RRab
V36	0.5413	0.545	0.276/0.244	RRab
V40	0.3853	0.38535	0.51895/0.18834	RRc, lower star Fig. 9, instrumental magnitudes
V43	0.3206	0.3211	0.3232/0.25286	RRc
V44	—	non-var		HB
V45	—	non-var		HB
V46	—	non-var		HB
V47	—	LP?		HB, next to overbright (possibly variable) stars
V48	—	LP?		HB
V50	—	non-var		HB
V51	—	LP?		HB, ≡S8 in Ref.2
V54	—	non-var		
V55	—	non-var		
V56	—	LP?		≡S72 (Ref. 2), RG, spectroscopic binary candidate (Ref. 3)
V57	—	non-var		
V58	—	non-var		
V59	—	non-var		≡S94 (Ref. 2)
V60	—	non-var		
V65	0.0872	non-var		
V70	0.3031	0.30315(9)	0.080/0.083	EB
V72	0.3084	0.30847	0.118/0.100	EB, BSS
V75	0.2973	non-var		
V76	0.3058	0.305736	0.29979/0.23335	RRc, $V12$ in ASAS Variable Stars Catalogue (Ref. 4)
V77	—	LPV?		possible EB (Ref. 1), spectroscopic binary candidate (Ref. 3), X-ray source associations: CX5 and CX9 (Ref. 5).
V78	—	non-var		
V79	1.2472	close to 1.2		very noisy light curve
V80	—	non-var		

Ref. 1. Stetson et al. 2014; Ref. 2. Stetson 2000; Ref. 3. Sommariva et al. 2009; Ref. 4. Pojmanski + 2002-2005; Ref. 5. Bassa et al. 2004, Kaluzny et al. 2013.

and I light curves. All these RR Lyrae do not belong to the M4 cluster and are the field variables. The distances to NV3 and C2 are estimated as 4.37 (Torrealba+ 2015) and 7.7 Kpc (Stetson et al. 2014). Two of the new RR Lyrae exhibit Blazhko modulation and for another one the data is insufficient to firmly determine the pulsation mode.

7.3.2. Eclipsing Binaries

We find eight eclipsing binaries; two of type EA (detached), five of the type EW (contact binaries) and one of EB/EW-type with period of ∼7.8 days – we cannot determine it more accurately as the interval of observations is shorter than the period. Of these binaries only NV4 is a cluster member and a possible BSS. Two of the EW binaries, NV11 and NV14, display O'Connell effect, where the primary and secondary maxima in the light curves have different magnitudes (Wilsey & Beaky 2009). One of the Algol-type variable, NV5, is also an X-ray source.

7.3.3. Other Types

We find four field cepheids: two of Delta Scuti type and two classical cepheids. Both of the classical cepheids are previously reported as X-ray sources (see next subsection). NV16 is a multiperiodic variable, therefore, we only show the time-domain light curve in R band in Fig. 10, *Right*.

We also have three unclassified variables: NV1,

Table 5: Data on new variables

ID	RA	DEC	PPMXL† μ_α, μ_δ	Period (day)	ΔR/ΔI (mag)	Epoch‡ 2455000.0+	GCVS Type/Comment
NV1	16:21:55.81	-26:13:29.0	-15.6, -6.8	≈33	0.105/0.063	846.9082	Unclassified LPV; could be 0.5046(?)
NV2	16:22:35.93	-26:19:37.2	-5.6, -6.9	46(1)	0.090/0.051	700.0000	LPV+linear trend -0.0009 mag d^{-1}; IR source 2MASS#J16223585-2619365, T-Tauri-like
NV3	16:25:29.222	-26:17:15.66	-6.1, -6.0	0.49178(3)	0.567/0.531	711.5392	RRab
NV4	16:25:09.48	-26:39:42.4	-26.5, -23.1	0.34444(1)	0.328/0.309	710.3406	EW
NV5	16:24:38.66	-26:44:24.1	-3.4, -9.9	0.54457(3)	0.406/0.403	711.3890	EA, ROSAT X-ray source[1]
NV6	16:24:44.27	-26:46:18.4	-12.4, -24.4	0.8613(1)	0.120/0.124	711.1503	Unclassified (P=0.4306?), HRV=-3.1[2]
NV7	16:21:47.46	-26:09:40.5	-6.8, -12.7	0.43031(1)	0.300/0.267	711.0751	RRc/RRab, Blazhko effect?
NV8	16:24:28.41	-26:28:28.1	-1.5, -11.8	0.64783(1)	0.190/0.150	712.4039	RRc
NV9	16:22:06.35	-26:39:25.8	-16.2, -11.6	7.8	0.335/0.274	715.4	EB/EW
NV10	16:20:51.18	-26:36:20.5	-15.2, -11.0	0.70777(6)	0.375/0.367	711.7192	RRab, Blazhko effect
NV11	16:20:49.93	-26:36:07.9	-9.7, -4.4	0.35640(5)	0.374/0.331	710.5815	EW, O'Connell effect
NV12	16:23:35.69	-26:47:45.8	-14.1, -17.8	3.944(2)	0.153/0.156	719.3348	DCEP? Associations: ROSAT X-ray source 1RXS J162336.6-264747[3] *Chandra* X-ray source CXOJ162335.5-264746[4]
NV13	16:21:26.04	-26:46:05.8	-12.5, -13.7	0.33604(1)	0.644/0.788	709.8105	RRab
NV14	16:24:59.14	-26:54:20.7	-4.4, -13.3	0.44726(2)	0.430/0.406	710.5156	EW, O'Connell effect
NV15	16:24:16.63	-26:57:14.0	-19.3, -32.1	5.091(3)	0.392/0.205	726.6111	DCEP?, HRV=-5km/sec^2, X-ray source 1RXS J162417.7-265717 at ∼ same location[3]
NV16*	16:22:57.80	-26:54:40.5	-10.59, 3.32				DSCT (multiperiodic):
				0.2477(1)	0.156	709.7545	P_1
				0.1579(1)	0.122	709.9546	P_2
				0.2114(4)	0.022	709.8627	P_3
NV17	1. 16:21:48.43	-26:50:55.0	-65, 64	1.3144(2)	0.203/0.062	713.2884	EA, Visual double star WDS J16218-2651
	2. 16:21:47.99	-26:50:47.2	-54, 66				+ high proper motion star [5]
NV18	16:22:50.63	-26:28:51.4	-32.4, -11.5	0.28054(1)	0.168/0.168	709.6490	EW, 3 close stars on C18 frames, coordinates of the most prob. one (PPMXL'10)
NV19	16:21:03.99	-26:24:35.9	-7.0, -3.0	0.226067(7)	0.138/0.138	710.7800	EW, 2 stars at 2.136″, no PPMXL, UCAC4 data, only UKIDSS#J162103.99-262435.9 and PM
NV20	16:21:05.83	-26:24:15.7	-8.2, -5.6	0.112966(3)	0.081/0.042	710.5573	DSCT
C2	16:24:07.59	-26:38:36.9	22, 9	0.45427(7)	0.835/0.645	711.3951	RRab

†M4 cluster overall proper motion (PPMXL 2010): $\mu_\alpha - 17.9$, $\mu_\delta = -19.4$.

‡Epochs are for minimum light for eclipsing binaries and maximum light for pulsating stars.

* Epochs, periods and amplitudes are only for R filter for this star.

References to the additional data: 1. M4 source#5, Ishikawa+ 2004; 2. Lane+ 2011; 3. Voges+ 2000; 4. Evans+ 2010; 5. Hartkopf+ 2013.

GCVS (General Catalog of Variable Stars, Samus+ 2007-2013) type are codified as follows: EW – W Ursae Majoris-type eclipsing variable; EA – Algol (Beta Persei)-type eclipsing system; DCEP – classical cepheid, or Delta Cep-type variable; DSCT – variable of the Delta Scuti type, field analog of SX Phe variables.

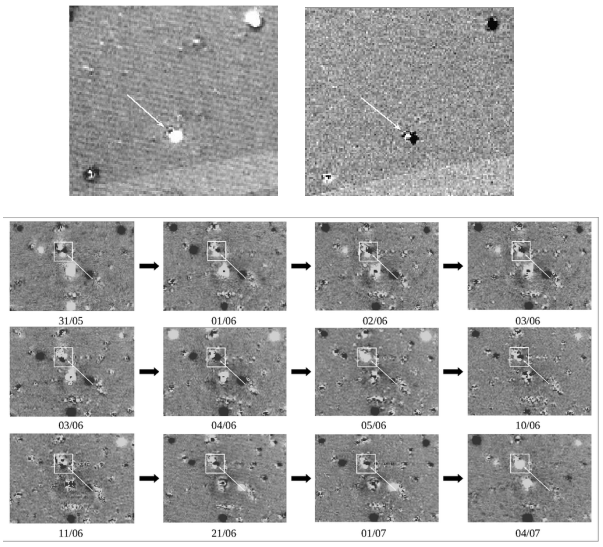

Fig. 9.— *Top*: T40 difference frames of V36 from two different nights. White arrow points to a pair of spatially close stars (3″.6 apart), the lower star is clearly a variable. *Bottom*: T40 difference frames of the V40 pair (in the white box) from 31st of May (31/05) onwards. It is clearly seen that both stars are variable. The angular separation is 1″.666. In the centre there is a saturated star. Other variables here are V16, V18, V21, V24 and V25.

NV2 and NV6. The first two are most probably long-period variables, where NV2 displays the light curve that resembles T-Tauri stars light curves. It is also a reported IR source, which then makes it possible for it to be a star belonging to the foreground Rho Ophiuchi star formation region. We present their time-domain light curves in both R and I filters in Fig. 10, *Left*.

7.3.4. The nature of variable NV12

This source is an unresolved extended image as it appears on the C18 frames (it is outside T40 FOV). At least three X-ray sources and several optical sources are listed within a 1′ radius circle in different catalogs (SIMBAD Astronomical Database). A Chandra point X-ray source CXOJ162335.5-264746 (Evans+ 2010) coincides with the position of the object. A ROSAT X-ray source 1RXSJ162336.6-264747 (Ueda+ 2001) is at ∼ 13.4″ to the left of it and an ASCA unresolved X-ray source 1AXGJ162334-2647 with the MEKAL fitted spectrum (Ueda+ 2001) at ∼ 13″ to the right of it. An archival red ESO/R/MAMA image (Fig. 12, *Left*) shows an extended object at this position. Imaging from 1.3-m JCBT telescope of the VBO (Vainu Bhappu Observatory, Tamil Nadu, India) resolves the object into an optical double star (Fig. 12,*Right*). The position of

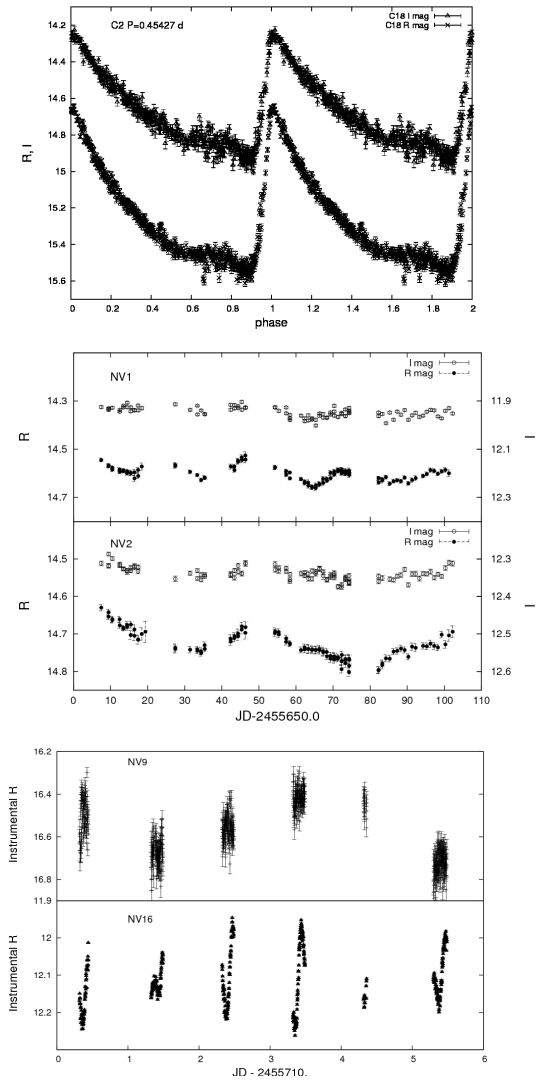

Fig. 10.— *Top*: C18 light curve of C2 in standard R and I magnitudes, phased with 0.45427(7) d period. *Middle*: T40 time-domain light curves of NV1 and NV2 in standard R and I magnitudes. *Bottom*: C18 time-domain light curves of NV9 and NV16 in instrumental R magnitudes.

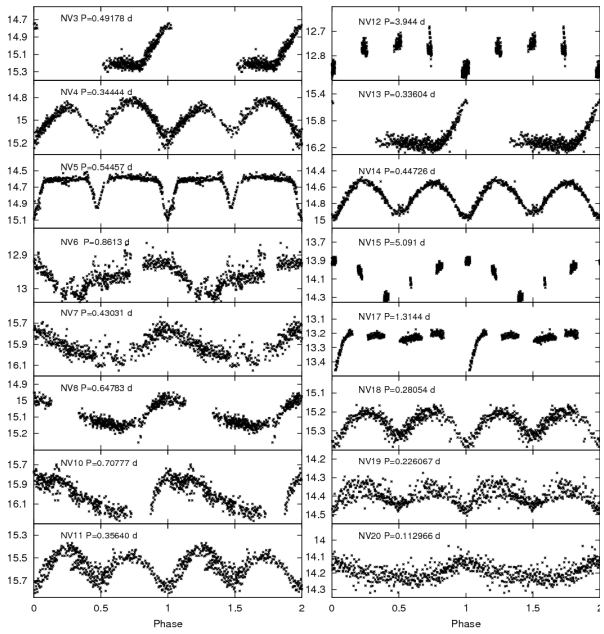

Fig. 11.— Phased light curves of new variables in instrumental R magnitudes. Names and periods are given in the plots.

the Chandra X-ray source CXOJ162335.5-264746 is coincident with the lowest of the two stars (see Table 5 and Fig. 12,*Right*). Our preliminary analysis indicates that this is probably a Delta Cep-type variable, or a classical cepheid, which were shown in 2009 (Engle et al. 2009) to display X-ray activity, representing the first true detection of X-ray emission in classical cepheids. Incidentally, another detected DCEP, NV15, also has an X-ray source association (Table 5). Spectroscopic studies of NV12 are underway and the results will be reported in a forthcoming paper.

7.4. Cluster membership of new variables

7.4.1. Proper Motion Diagram

One of the way to detect foreground/background contamination consists in identifying field stars on the basis of their proper motion which usually differs from the overall cluster motion. On the vector point diagram (VPD), the zero point of the motion is the mean motion of the cluster itself, and the bulk of the stars clustered around the origin would consist mostly of cluster members, while field stars will be distributed over a larger range of proper

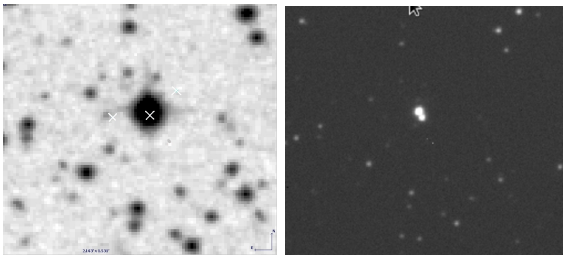

Fig. 12.— The field of NV12:*Left*: Archival ESO/R/MAMA image of the field. The object is in the centre. White crosses indicate the associated X-ray sources: CXOJ162335.5-264746 right on the object; 1RXS J162336.6-264747 to the left of it and 1AXGJ162334-2647 to the right. *Right*: 30-sec V-band JCBT image shows the object to be a visual double star with $\sim 2''.9$ separation. The variable is most probably the lower star.

motions. To build the VPD for our sample, we have found the PPMXL 2010 proper motion for all stars in quad 8 as well as for our newly found variables. The VPD of Fig. 13 shows that majority of the stars in quad 8 share the mean cluster motion. It also shows that most of the newfound variables are not cluster members. The possible members among the new ones are NV4, NV6, NV9, NV10, NV12 and NV13, and most certain non-members are NV17, NV18, NV19 and C2.

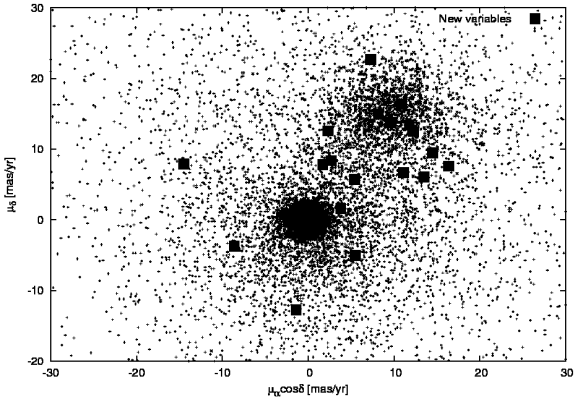

Fig. 13.— Vector point diagram, in equatorial coordinates, for all stars in quad 8 with available measures of proper motions (PPMXL'12). Filled squares are the newly found variables.

7.4.2. Colour-Magnitude Diagram

To aid in identification of the newly found variables, we have constructed the CMD of the central region of M4 from C18 images (Fig. 14). The RF of subsection 4_3 was astrometrically and photometrically calibrated (see Sec. 6). In Fig. 14 we present the CMD with known variables located in this subsection; the isochrone from Girardi et al. (2000) for an age of 12.6 Gyr in absolute magnitudes is superimposed on the plot. From the sliding fit, we obtain $E(R-I) = 0.22$, corresponding to the reddening $E(B-V) = 0.27$, where total extinction in R and I bands $A_R = 2.32\,E(B-V)$ and $A_I = 1.5\,E(B-V)$, respectively, were taken from Schultz & Wiemer (1975). The distance modulus 11.27 was calculated for the distance of 1.8 Kpc to M4 (e.g. Kaluzny et al. 2013). This curve matches the colours of the turnoff.

Based on the CMD, we find that out of NV4, NV6, NV9, NV10, NV12 and NV13, only NV4 (an EW star located close to the BSS region) can be firmly considered as cluster member, with the rest most probably being foreground/background objects. However, NV12 is still a subject of a study. It is possible that its C18 magnitude and colours are blended, since on C18 we could not resolve the two components.

7.5. Candidate variables

We have selected few possible variables, whose light curves however are either noisy or the stars themselves are situated on the edges, where the apparent variability could have been induced artificially. For all but two we have the light curves from both telescopes. We have assigned the name VC (variable candidate) to these stars. The available data on these stars and their time-domain light curves are presented in Table 6 and Fig. 15, respectively.

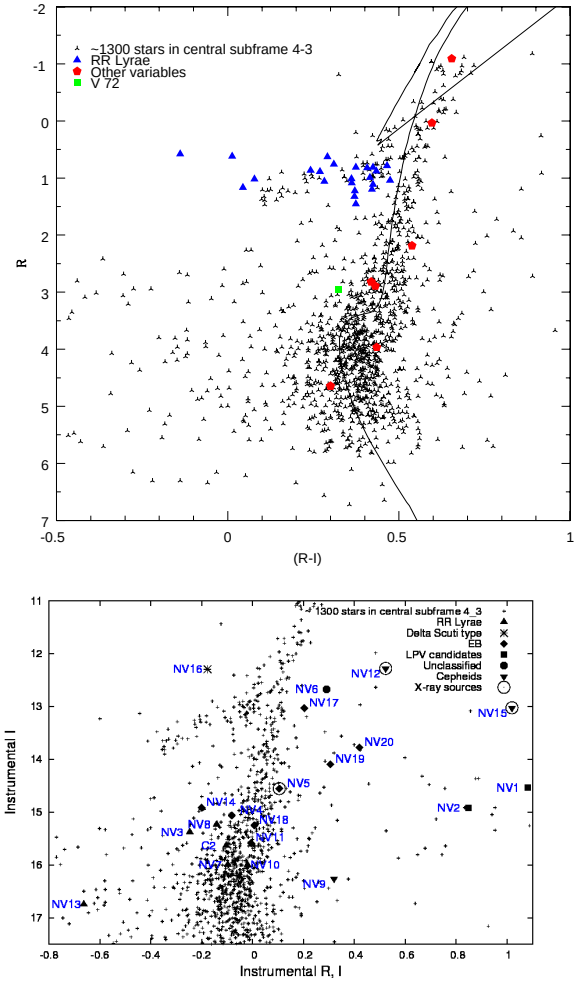

Fig. 14.— *Top*: CMD of the 4_3 subframe of C18 central part of M4 in absolute magnitudes with known RR Lyrae and other variables located in this subframe. V72 is the BSS eclipsing binary star located in the BSS region of the CMD. Overplotted is a 12.6 Gyr isochrone from Girardi et al. (2000) with $E(B-V) = 0.27$. *Bottom*: CMD in instrumental magnitudes of the 4_3 subframe of C18 central part of M4 with newly found variables. Location on the CMD aids in variables identification.

8. Conclusions

Globular cluster M4 was observed as part of our multi-site program on the search of low-mass objects in globular cluster by microlensing. We presented here the results of 2011 observational run on two Wise Observatory (Tel Aviv, Israel) telescopes. We did not detect any variability signal that could be interpreted as a ML event with photometric depth larger than 0.1 mag. Most important factor in our data set that strongly limited the ML detection is a poor sampling cadence

Table 6: Data on candidate variables

ID	RA	DEC	UCAC4#[1]	PPMXL μ_α, μ_δ	Type	Additional data
VC1	16:22:20.0	-26:32:38.6	318-087831	$-10.6, -1.6$	LPV/EB	
VC2	16:22:34.8	-26:27:13.1	318-087877	$-5.0, -20.5$	LPV/EB	Associations: CXO J162234.8-262712,[2] X-ray/Radio source[3]
VC3	16:22:22.9	-26:24:01.9	318-087841	$-6.3, 0.6$		
VC4	16:22:41.35	-26:26:02.5	318-087915	$-3.0, -2.0$	LPV?	≡S989[4],2MASSJ162241.4-262601 IR source[5]
VC5	16:23:33.14	-26:30:56.8	318-088763	$-6.7, 41.9$		no PPMXL data, PM from UCAC4
VC6	16:22:41.54	-26:23:03.4	319-085449	$-28.4, -24.9$		
VC7	16:22:18.00	-26:29:11.6	no data	$-8.7, -4.8$		3 stars close, PPMXL data only on one star.

1. Zacharias+ 2013; 2. Evans+ 2010; 3. Flesh 2010; 4. Stetson 2000; 5. Evans+, 2003, c2d Spitzer final data release (DR4).

of observations rather than photometric limitations. Our initial proposal to obtain several datapoints a night was not realized due to various factors, weather, malfunctions, clashes with other programs, etc. It is entirely possible that we have missed the event since the calculated time-scale due to the FFP is of the order of a day, therefore the statistical significance of the null detection is very low. Though no definitive ML signal was detected, we have obtained a good R and I photometry of an M4 field. We have recovered most of the variables previously reported in M4. We found the coordinates of the stars for which there was no data in Clement's catalog. We have inspected previously suspected field variable V12 (ASAS) and have identified it with the catalogued V76, obtaining its R and I light curves. We have confirmed that two previously suspected SX Phe stars in M4 do not pulsate as SX Phe, and that M4 is still void of SX Phe stars. We also obtained R and I photometry of variables not covered by Stetson et al. (2014) work: V3, V34 and V43. We concur with Stetson et al. (2014) conclusion that previously reported as variable, stars V57–V60, V65, V75 and V80, are non-variable in both our sets to the limit of our sensitivity. However, stars V70 and V72, that appear to be non-variable in their data, are in, fact variable, and one of them is a BSS.

Our survey resulted in detection of several new variables and variable candidates. Out of twenty new certain variables, however, only one (NV4) can be accepted as a cluster member based on its proper motion and a CMD location. It is an eclipsing binary and also most probably a blue straggler. We have detected seven RR Lyrae: 2 RRc, 4 RRab and one whose pulsation mode cannot be yet determined based on incompleteness of our light curve. One of these RR Lyrae, C2, was previously also discovered by Stetson et al. (2014), though we complement their data with R and I light curves. Some of the new variables are associated with X-ray/radio sources, one of them is Algol-type and two are probable classical cepheids. We also have detected seven candidate variables, where variability cannot be fully confirmed on the basis of only our data. These candidates are, however, look variable in the Catalina Sky Survey online data as well (except VC5, which was not covered), but insufficient CSS temporal coverage there does not allow to firmly define the periods. We are looking closely into the nature of a new variable NV12, which is associated with X-ray sources reported previously by three different missions. The results of our spectroscopic investigations will be reported in a separate communication.

All our R and I light curves for previously known variables can contribute to the completeness of the variable stars database of M4, which has been started by the team Stetson et al. (2014). Our calibrated photometry for these stars, their coordinates and light curves will be available on our web site and/or upon request. It is our hope that a full and complete long-baseline photometric database can be established for the nearest to us globular cluster.

We are grateful to Wojtek Pych for providing us with the modified version of DIAPL and for his continuous help and support in its running. This research used the facilities of the Canadian

Astronomy Data Centre operated by the National Research Council of Canada with the support of the Canadian Space Agency.

REFERENCES

Adamów, M., Niedzielski, A., Villaver, E., Nowak, G., & Wolszczan, A. 2012, ApJ, 754, LL15

Adams, F. C., Hollenbach, D., Laughlin, G., & Gorti, U. 2004, ApJ, 611, 360

Alard, C., & Lupton, R. H. 1998, ApJ, 503, 325

Alcaino, G. 1975, A&AS, 21, 5

Alcock, C., Allsman, R. A., Alves, D., et al. 1995, ApJ, 454, L125

Allen, C., & Santillan, A. 1993, Revista Mexicana de Astronomia y Astrofisica, 25, 39

Anglada-Escudé, G., Arriagada, P., Tuomi, M., et al. 2014, MNRAS, 443, L89

Bally, J. 2003, 287, 263

Baumeister, H., Afonso, C., Marien, K.-H., & Klein, R. 2006, Proc. SPIE, 6269, 62693I

Beer, M. E., King, A. R., & Pringle, J. E. 2004, MNRAS, 355, 1244 Evans, N. J., II, Allen, L. E., Blake, G. A., et al. 2003, Publ. Astron. Soc. Pac., 115, 965

Bennett, D. P., Anderson, J., Beaulieu, J., et al., 2007, arXiv:0704.0454 (White Paper Submitted to the NASA/NSF Exoplanet Task Force)

Bennet, D. P. et al. 2010, in 'Completing the Census of Exoplanets with the Microlensing Planet Finder (MPF)', RFI Response for the Astro2010 Program Prioritization Panel, (The Basis for the Exoplanet Program of the WFIRST Mission), arXiv:1012.4486 [astro-ph.EP].

Bonnarel, F., Fernique, P., Bienaymé, O., et al. 2000, A&AS, 143, 33

Brosch, N., Polishook, D., Shporer, A., et al. 2008, Ap&SS, 314, 163

Buchhave, L. A., Latham, D. W., Johansen, A., et al. 2012, Nature, 486, 375

Campante, T. L., Barclay, T., Swift, J. J., et al. 2015, ApJ, 799, 170

Cassan, A., Kubas, D., Beaulieu, J.-P., et al. 2012, Nature, 481, 167

Chatterjee, S. et al, 2012, MNRAS, 427, 1587

Clement, C. M., et al. 2001, AJ, 122, 2587

Dado, S., Dar, A., & Ribak, E. 2011, arXiv:1102.2622

Davies, M. B and Sigurdsson, S., 2001, MNRAS, 324, 612.

Delorme, P., Gagné, J., Malo, L., et al. 2012, A&A, 548, AA26

Del Santo, M., Nucita, A. A., Lodato, G., et al. 2014, MNRAS, 444, 93

de Luca, F., & Jetzer, P. 2008, International Journal of Modern Physics D, 17, 2305

Di Folco, E., Dutrey, A., Guilloteau, S., et al. 2014, SF2A-2014: Proc. Annual meeting of the French Society of Astronomy and Astrophysics, 135

Durand-Manterola, H. J. 2010, arXiv:1010.2735

Engle, S. G., Guinan, E., Evans, N., & DePasquale, J. 2009, Bulletin of the American Astronomical Society, 41, #433.12

Evans, N. J., II, Allen, L. E., Blake, G. A., et al. 2003, Publ. Astron. Soc. Pac., 115, 965

Evans, I. N., Primini, F. A., Glotfelty, K. J. et al. 2010, ApJS, 189, 37E

Flesch, E. 2010, PASA, 27, 283

Fregeau, J. M., Joshi, K. J., Portegies Zwart, S. F., & Rasio, F. A. 2002, ApJ, 570, 171

Ford, Eric B., 2014, PNAS, 111, 12616

Fukugita, M., & Peebles, P. J. E. 2004, ApJ, 616, 643

Gaudi, B. S., Bennett, D. P., Udalski, A., et al. 2008, Science, 319, 927

Gibson, C. H., & Schild, R. E. 1999, arXiv:astro-ph/9904362

Gilliland, R. L., Brown, T. M., Guhathakurta, P., et al. 2000, ApJ, 545, L47

Girardi, L., Bressan, A., Bertelli, G., & Chiosi, C. 2000, A&AS, 141, 371

Gorbikov, E., Brosch, N., & Afonso, C. 2010, Ap&SS, 326, 203

Gould, A. 1992, ApJ, 392, 442

Greenstein, J. L. 1939, ApJ, 90, 387

Hartkopf, W. I., Mason, B. D., Finch, C. T., et al. 2013, AJ, 146, 76

Hartman, J. D., Gaudi, B. S., Holman, M. J., et al. 2008, ApJ, 675, 1254

Horch, E. P., Howell, S. B., Everett, M. E., & Ciardi, D. R. 2014, ApJ, 795, 60

Hurley, J. R., & Shara, M. M. 2001, Bulletin of the American Astronomical Society, 33, 1410

Hurley, J. R., & Shara, M. M. 2002, ApJ, 565, 1251

Ida, S.,& Kokubo, E. 2002, in "Planetary Systems in the Universe: Observation, Formation and Evolution", ed. A. J. Penny, P. Artymowicz, A.-M. Lagrange, & S. S. Russell (San Francisco: ASP), IAU Symp., 202.

Ishikawa, T., Ishida, M., Ishisaki, T., Ohashi, T. and Yamasaki, N.Y. Publ. Astron. Soc. Jpn., 2004, 56, 453

Jetzer, P., Straessle, M., & Wandeler, U. 1998, A&A, 336, 411

Jetzer, P. 2015, XIII Marcel Grossmann Meeting: On Recent Developments in Theoretical and Experimental General Relativity, Astrophysics and Relativistic Field Theories, 2075

Kaluzny, J., Thompson, I. B., & Krzeminski, W. 1997, AJ, 113, 2219

Kaluzny, J., Thompson, I. B., Rozyczka, M., & Krzeminski, W. 2013, Acta Astronomica, 63, 181

Lafler, J., & Kinman, T. D. 1965, ApJS, 11, 216

Lane, R. R., Kiss, L. L., Lewis, G. F., et al. 2010, MNRAS, 406, 2732

Lane, R. R., et al. 2011, A&A,530, 31L

Leon, S., Meylan, G., & Combes, F. 2000, A&A, 359, 907

Leonard, P. J. T., Richer, H. B., & Fahlman, G. G. 1992, AJ, 104, 2104

Lin, D. N. C., Laughlin, G., Bodenheimer, P., & Rozyczka, M. 1998, Science, 281, 2025

Liu, M. C., Magnier, E. A., Deacon, N. R., et al. 2013, ApJ, 777, LL20

Maciejewski, G. 2005, PERSEA 2.01, Period Search Program for Windows. (http://www.astri.umk.pl/ gm/SAVS/)

Meibom, S., Torres, G., Fressin, F., et al. 2013, Nature, 499, 55

Mochejska, B. J., Kaluzny, J., Thompson, I., & Pych, W. 2002, AJ, 124, 1486

Mochejska, B. J., Stanek, K. Z., Sasselov, D. D., et al. 2006, AJ, 131, 1090

Monaco, L., Villanova, S., Bonifacio, P., et al. 2012, A&A, 539, AA157

Montalto, M., Villanova, S., Koppenhoefer, J., et al. 2011, A&A, 535, AA39

Nascimbeni, V., Bedin, L. R., Piotto, G., De Marchi, F., & Rich, R. M. 2012, A&A, 541, AA144

Nascimbeni, V., Bedin, L. R., Heggie, D. C., et al. 2014, MNRAS, 442, 2381

Nucita, A. A., De Paolis, F., Ingrosso, G., et al. 2006, ApJ, 651, 1092

Paczyński, B. 1994, Acta Astron., 44, 235

Peña Ramírez, K., Béjar, V. J. S., Zapatero Osorio, M. R., Petr-Gotzens, M. G., & Martín, E. L. 2012, ApJ, 754, 30

Pojmanski, G., Maciejewski, G., Pilecki, B., & Szczygiel, D. 2006, VizieR Online Data Catalog, 2264, 0

Rattenbury, N. J., & Mao, S. 2006, MNRAS, 365, 792

Richer, H. B., Ibata, R., Fahlman, G. G., & Huber, M. 2003, ApJ, 597, L45

Richer, H. B., Fahlman, G. G., Brewer, J., et al. 2004, AJ, 127, 2771

Roberts, L. C., Jr., Tokovinin, A., Mason, B. D., et al. 2015, AJ, 149, 118

Roell, T., Neuhäuser, R., Seifahrt, A., & Mugrauer, M. 2012, A&A, 542, AA92

Röser, S., Demleitner, M., & Schilbach, E. 2010, AJ, 139, 2440

Rosotti, G. P., Dale, J. E., de Juan Ovelar, M., et al. 2014, MNRAS, 441, 2094

Safonova, M., & Stalin, C. S. 2010, New A, 15, 450

Samus, N. N., Durlevich, O. V., & et al. 2009, VizieR Online Data Catalog, 1, 2025

Samus N.N., Durlevich O.V., Kazarovets E V., Kireeva N.N., Pastukhova E.N., Zharova A.V., et al. General Catalog of Variable Stars (GCVS database, Version 2012Apr), (Samus+ 2007-2013), VizieR On-line Data Catalog: B/gcvs

Schultz, G.V., & Wiemer, W. 1975, A&A, 43, 133.

Skrutskie, M. F., Cutri, R. M., Stiening, R., et al. 2006, AJ, 131, 1163

Soker, N., & Hershenhorn, A. 2007, MNRAS, 381, 334

Sommariva, V., Piotto, G., Rejkuba, M., et al. 2009, A&A, 493, 947

Spurzem, R., Giersz, M., Heggie, D. C., & Lin, D. N. C. 2009, ApJ, 697, 458

Stevenson, D.J. 1998, Nature, 392, 497

Stetson, P. B. 2000, PASP, 112, 925

Stetson, P. B., Braga, V. F., Dall'Ora, M., et al. 2014, PASP, 126, 521

Strigari, L. E., Barnabè, M., Marshall, P. J., & Blandford, R. D. 2012, MNRAS, 423, 1856

Soker, N., & Hadar, R. 2001, MNRAS, 324, 213

Sumi, T., Kamiya, K., Bennett, D. P., et al. 2011, Nature, 473, 349

Sutherland, W. 1999, Reviews of Modern Physics, 71, 421

Veras, D., & Raymond, S. N. 2012, MNRAS, 421, L117

Veras, D., Wyatt, M. C., Mustill, A. J., Bonsor, A., & Eldridge, J. J. 2011, MNRAS, 417, 2014

Voges, W., Aschenbach, B., Boller, T., et al. 2000, VizieR Online Data Catalog, 9029, 0

Ueda, Y., Ishisaki, Y., Takahashi, T., Makishima, K., & Ohashi, T. 2001, ApJS, 133, 1

Weldrake, D. T. F., Sackett, P. D., & Bridges, T. J. 2007, Transiting Extrapolar Planets Workshop, 366, 289

Weldrake, D. T. F., Sackett, P. D., & Bridges, T. J. 2008, ApJ, 674, 1117

Wilsey, N. J., & Beaky, M. M. 2009, Society for Astronomical Sciences Annual Symposium, 28, 107

Wozniak, P. R. 2000, Acta Astron., 50, 421

Wylie-de Boer, E., Freeman, K., & Williams, M. 2010, AJ, 139, 636

Zacharias N., Finch C.T., Girard T.M., Henden A., Bartlett J.L., Monet D.G., Zacharias M.I. 2013, AJ, 145, 44

Zapatero Osorio, M. R., Béjar, V. J. S., Martín, E. L., et al. 2000, Science, 290, 103

Zubovas, K., Nayakshin, S., & Markoff, S. 2012, MNRAS, 421, 1315

This 2-column preprint was prepared with the AAS LaTeX macros v5.2.

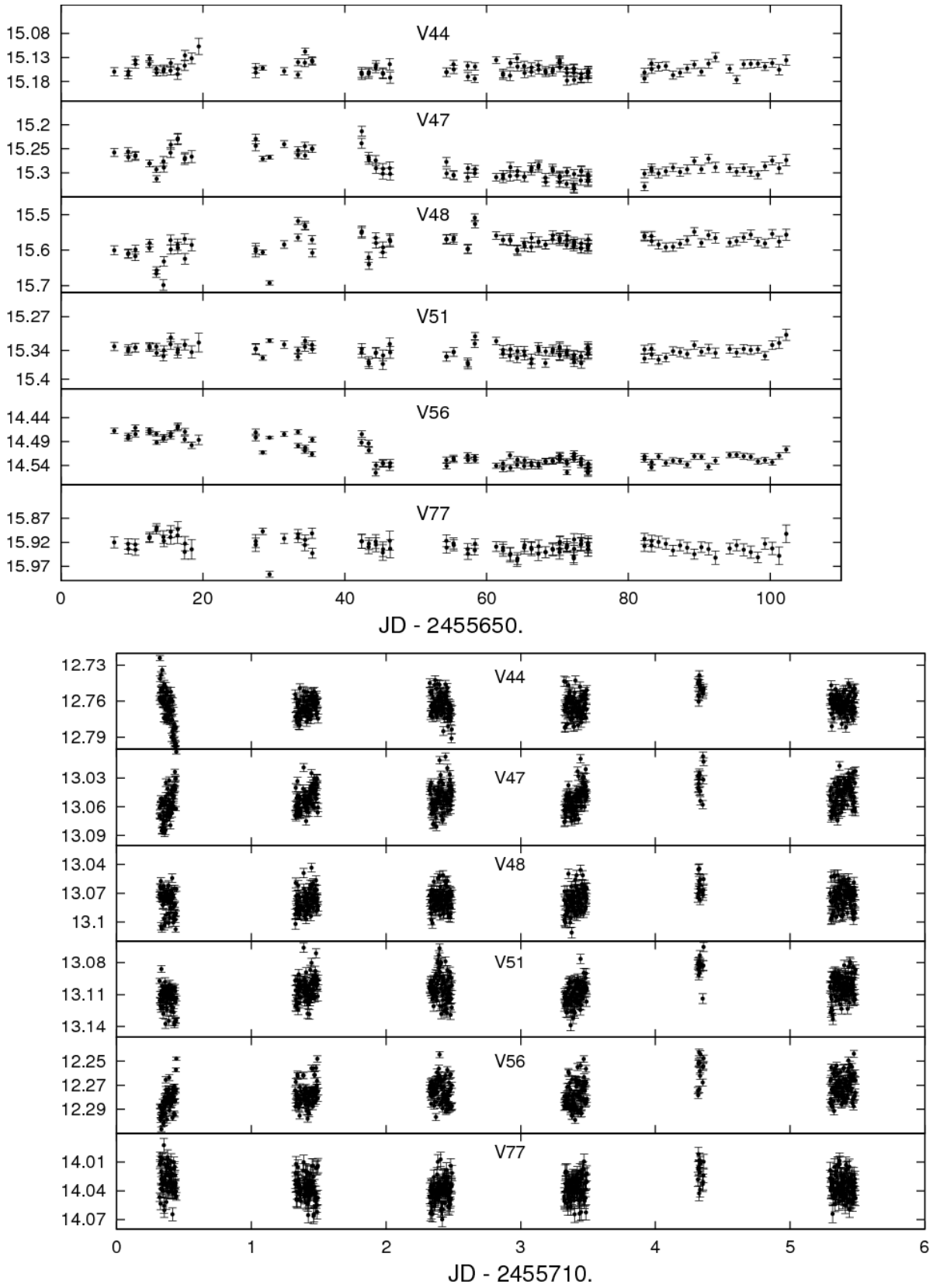

Fig. 5.— T40 (*Left*) and C18 (*Right* time-domain light curves of variables V44, V47, V48, V51, V56 and V77 in instrumental R magnitude. Names are given in the plots.

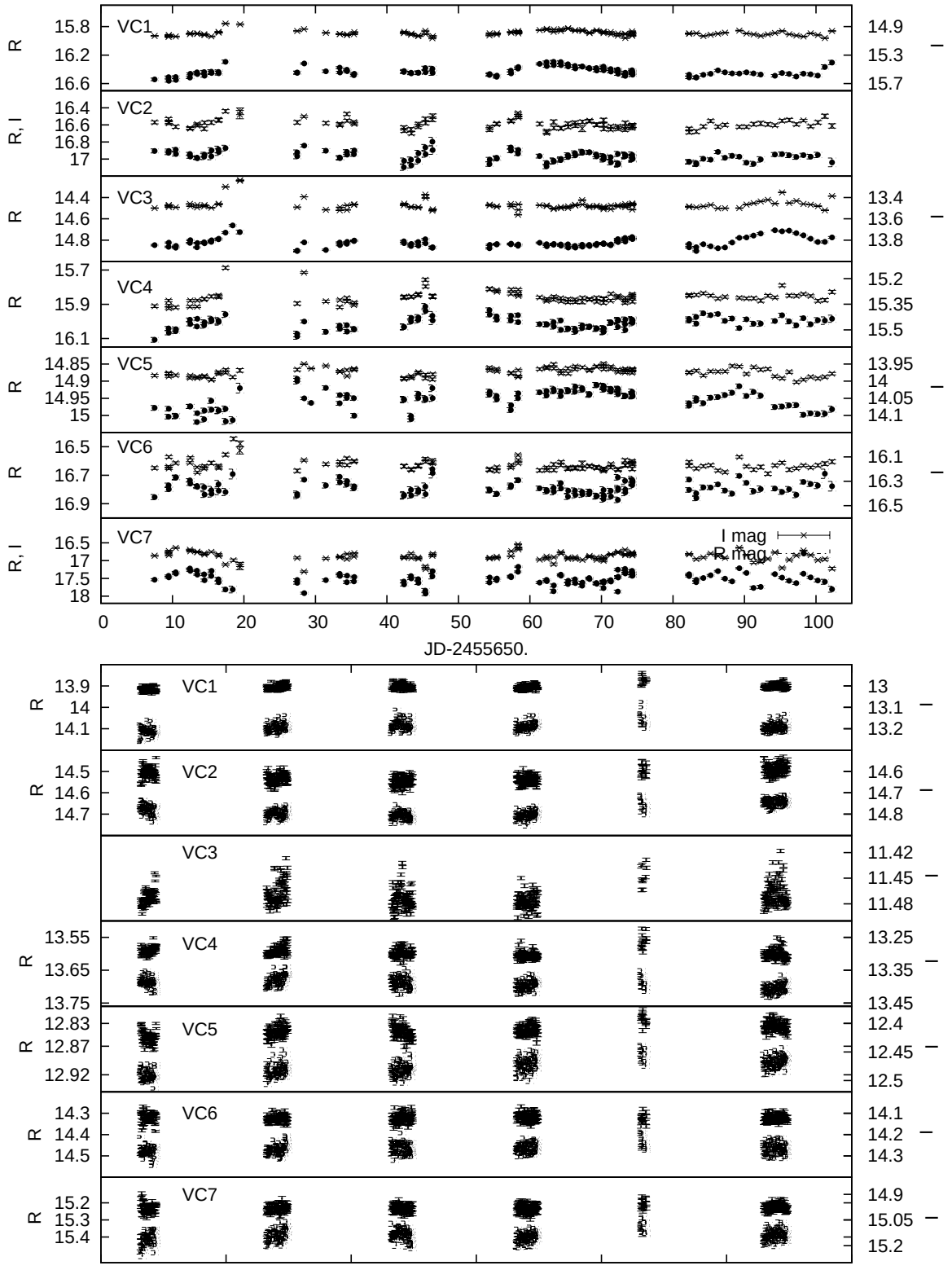

Fig. 15.— Time-domain light curves of candidate variables. *Left*: T40 light curves; *Right*: C18 light curves.